Journal of Materials Chemistry A

ROYAL SOCIETY OF CHEMISTRY

COMMUNICATION

View Article Online
View Journal | View Issue

Published on 31 January 2020. Downloaded by Lawrence Berkeley National Laboratory on 3/13/2020 3:43:11 PM.

Check for updates

Cite this: *J. Mater. Chem. A*, 2020, **8**, 4239

Received 18th December 2019
Accepted 29th January 2020

DOI: 10.1039/c9ta13829c

rsc.li/materials-a

Combinatorial screening yields discovery of 29 metal oxide photoanodes for solar fuel generation†

Lan Zhou,[a] Aniketa Shinde,[a] Dan Guevarra,[a] Matthias H. Richter,[ab] Helge S. Stein,[a] Yu Wang,[a] Paul F. Newhouse,[a] Kristin A. Persson[cde] and John M. Gregoire *[af]

Combinatorial synthesis combined with high throughput electrochemistry enabled discovery of 29 ternary oxide photoanodes, 15 with visible light response for oxygen evolution. $Y_3Fe_5O_{12}$ and trigonal V_2CoO_6 emerge as particularly promising candidates due to their photorepsonse at sub-2.4 eV illumination.

Solar fuel generation from H_2O, CO_2 and sunlight comprises a promising renewable energy technology whose future proliferation relies on materials advancements, including identification of a photoanode for the oxygen evolution reaction (OER). A water-oxidizing photoanode can be coupled to a (photo) cathode for scalable generation of H_2 and C-containing fuels.[1] Metal oxides are the most extensively studied class of OER photoanode materials due to the availability of a multitude of metal oxide phases that may stably operate in the oxidative electrochemical environment while converting solar to photoelectrochemical (PEC) energy.[2–4]

In addition to historic efforts in developing the binary oxides α-Fe_2O_3, TiO_2 and WO_3 as solar fuels photoanodes, there have been concerted efforts to both explore modes of optimization and understand limiting factors for ternary oxides, most notably $BiVO_4$ (ref. 2) and also $ZnFe_2O_4$,[5] α-$SnWO_4$,[6] and copper vanadates.[7] high throughput (HiTp) experimental screening of OER photoanodes, pioneered by Parkinson[8,9] and McFarland[10] and advanced by others,[11–13] has accelerated exploration of photoanode candidates. The HiTp techniques described in the present work were previously deployed under guidance from first principles density functional theory (DFT) calculations, resulting in the discovery of β-$Mn_2V_2O_7$ (ref. 14) followed by 8 additional ternary metal vanadates[15,16] and 5 additional ternary metal manganates.[17] The present work includes ancillary discoveries from this theory-guided work as well as experimental discoveries from screening of composition spaces selected from literature precedent and/or intuition.

Recent reviews of solar fuels photoanodes have highlighted the dearth of metal oxides that operate over a sizable fraction of the solar spectrum, in particular below 2.4 eV, the photon energy onset for $BiVO_4$.[2–4] Herein we report photoactivity of 29 photoanode phases, 15 of which have visible light response and 5 are particularly promising due to the observation of photocurrent at or below 2.4 eV. The measured photocurrents are for non-optimized thin film samples within combinatorial libraries, motivating further development to achieve efficient utilization of the solar spectrum.

The HiTp experimental methods have been described previously and are further detailed in the ESI.† Briefly, for a given pair of elements, a compositionally graded film is deposited by co-sputter deposition in 6 mTorr of either Ar or mixed Ar/O_2, typically resulting in cation variation from *ca.* 20% to 80% across a 100 mm diameter Si (with Pt conducting layer) or glass (Pyrex or soda lime glass with SnO_2:F conducting layer) substrate. A series of 10–20 locations along each pseudo-binary composition gradient were chosen for characterization *via* a range of experimental techniques, each with a measurement spot size near or below 2 mm in diameter. Each of the selected locations comprises a thin film sample with approximately uniform composition, and the series of sample provides a composition grid for property measurements. Automated serial experimentation includes measurement of composition (X-ray fluorescence, XRF), crystal structure (X-ray diffraction, XRD), optical absorption (ultraviolet-visible spectroscopy, UV-vis), and photoelectrochemical activity (toggled illumination

[a]Joint Center for Artificial Photosynthesis, California Institute of Technology, Pasadena, California 91125, USA. E-mail: gregoire@caltech.edu

[b]Division of Chemistry and Chemical Engineering, California Institute of Technology, Pasadena, CA 91125, USA

[c]Joint Center for Artificial Photosynthesis, Lawrence Berkeley National Laboratory, Berkeley, CA 94720, USA

[d]Department of Materials Science and Engineering, University of California, Berkeley, CA 94720, USA

[e]Environmental Energy Technologies Division, Lawrence Berkeley National Laboratory, USA

[f]Division of Engineering and Applied Science, California Institute of Technology, Pasadena, CA 91125, USA

† Electronic supplementary information (ESI) available: Additional data tables, figures, and experiment details. See DOI: 10.1039/c9ta13829c

Published on 31 January 2020. Downloaded by Lawrence Berkeley National Laboratory on 3/13/2020 3:43:11 PM.

scanning droplet cell, SDC). The 1-dimensional composition gradient on a 2-dimensional substrate also provides nominally duplicate samples that can be evaluated for reproducibility and/or under different electrochemical conditions, such as different electrolyte pH.

Mining the photoanode experiments in the materials experiments and analysis database (MEAD)[18] resulted in enumeration of the 29 metal oxide phases in Table 1 (XRD-based phase identification summarized in Fig. S5†), which to the best of our knowledge have not been reported as photoanodes. Of these, 27 are ternary metal vanadates or manganates related to the computational screening of ref. 15, 16 and 17 which were not identified by these prior efforts due to absence of the phase in the Materials Project, unavailability of a band gap energy, or a calculated decomposition energy beyond the threshold of the respective screening pipeline. We note that this compendium of materials can guide development of a set of necessary and sufficient screening criteria based on computation of various structural, electronic, *etc.* properties. Of particular importance is characterization of the balance of accurate *vs.* inexpensive band gap calculations to enable accelerated, accurate screening, which is the topic of ongoing work. The other 2 are $YFeO_3$-orth, which is a polytype of the hexagonal structure that was previously reported,[19] and yttrium iron garnet ($Y_3Fe_5O_{12}$).

The photoanodes in Table 1 are sorted by our assessment of their propensity to be photoactive over the visible spectrum. The highest energy LED where photocurrent was not observed (where applicable) and the lowest energy LED where photocurrent was observed is noted, which places a lower and upper limit, respectively, on the photon energy onset of photocurrent. The upper limit is in the visible range for the first 15 phases, demonstrating their visible light response.

The first 5 photoanodes in Table 1 have some photoresponse at 2.07 eV but sustained photocurrent near or below the detectability limit, indicating that the onset for photocurrent is near this photon energy. Among these, $Y_3Fe_5O_{12}$ and V_2CoO_6-tri‡ are the most photoactive, motivating further exploration of their experimental data in Fig. 1 and 2, respectively. The PEC data for the other 3 phases are provided in Fig. S2.†

Table 1 Summary of 29 photoanodes discovered in the present work. The first 15 are designated as visible light photoanodes, 5 with photocurrent onset near 2.07 and 9 with photocurrent onset between 2.41 and 2.75 eV. The 9 phases with no lower limit for photocurrent onset were measured only with the 3.2 eV LED and may exhibit visible light photoactivity. The DFT band gap energy (typically lower than experiment value) using standard MP settings for structure relaxation and subsequent static calculation is shown where available. The electrolyte pH of the corresponding measurements is noted, and any additional electrolyte pH where photoactivity was observed is noted

		Limits on photon energy onset of photocurrent (eV)				Electrolyte pH	
Phase name	mp-id	Lower limit ($J = 0$)	Upper limit ($J > 0$)	UV-vis band gap (eV)	Computed band gap (eV)	Discovery experiments	Other pH with photoactivity
$Y_3Fe_5O_{12}$	19648	$\lesssim$2.07	2.41		N/A	13	10
V_2CoO_6-tri	622217	$\lesssim$2.07	2.41		1.58	9	
$YMnO_3$-hex	19227	$\lesssim$2.07	2.41		N/A	13	10
YMn_2O_5	542867	$\lesssim$2.07	2.41	2.5	1.07	10	
$YFeO_3$-orth	24999	2.07	2.41		1.56	13	10
$CaMnO_3$	19201	2.41	2.75	1.41	N/A	13	10
$V(Bi_5O_8)_5$	None	2.41	2.75		N/A	9	
$Nb_{10.7}V_{2.38}O_{32.7}$	None	2.41	2.75		N/A	9	
$NbVO_5$	769890	2.41	2.75		1.89	9	
$V_2Pb_4O_9$	647385	2.41	2.75		N/A	9	
V_2ZnO_6	551601	2.41	2.75		N/A	9	
$V_{4.51}Pb_{3.5}O_{14.75}$	None	2.41	2.75		N/A	9	
β-$VAgO_3$	566337	2.41	2.75		N/A	9	
$V_2Ag_{0.33}O_5$	None	2.41	2.75	2.5	N/A	9	
Ca_2MnO_4	19050	2.41	2.75	1.79	0.37	10	
Mn_7SiO_{12}	19650		3.2	1.9	N/A	13	
$YMnO_3$-orth	25025		3.2	2.3	0.41	13	10
$Mn_{(2/3)}Sb_{(4/3)}O_4$	763546		3.2		0.0	0	13
$Ca_2V_2O_7$	32434		3.2		3.05	9	
$CaMn_3O_6$	566229		3.2		N/A	10	13
Mg_6MnO_8	19239		3.2		2.29	10	
$SrMn_3O_6$	None		3.2		N/A	10	
$MnGeO_3$	643577		3.2		N/A	13	
$V_2Bi_8O_{17}$	None		3.2		N/A	9	
$V_2Bi_{12}O_{23}$	None	2.75	3.2	2.3	N/A	9	
$TaVO_5$	32407	2.75	3.2		2.17	9	
$V_2Pb_2O_7$	25796	2.75	3.2		2.87	9	
$V_2Zn_4O_9$	504923	2.75	3.2		2.55	9	
ZrV_2O_7	565725	2.75	3.2		2.59	9	

 This journal is © The Royal Society of Chemistry 2020

Published on 31 January 2020. Downloaded by Lawrence Berkeley National Laboratory on 3/13/2020 3:43:11 PM.

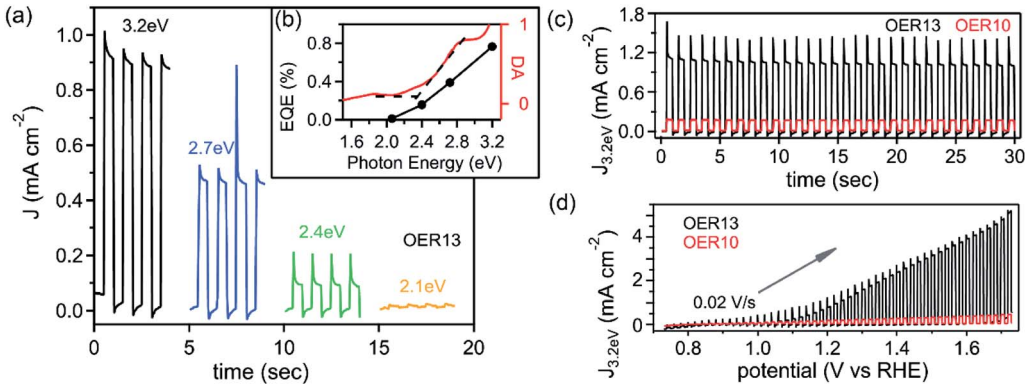

Fig. 1 Summary of toggled illumination PEC experiments on $Y_3Fe_5O_{12}$ where transition to higher (lower) current corresponds to toggling illumination on (off). (a) CA at 1.23 V *vs.* RHE in pH 13 electrolyte with 4 different light sources. (b) The corresponding spectral EQE (left axis) along with the UV-vis direct-allowed Tauc plot (right axis). Nominally duplicate samples were used to compare activity in pH 10 and pH 13 electrolytes, including (c) 30 s CA at 1.23 V *vs.* RHE and (d) CV with 3.2 eV illumination.

PEC characterization of $Y_3Fe_5O_{12}$ (Fig. 1) demonstrates photoactivity in pH 10 electrolyte and substantially higher photocurrent in pH 13 electrolyte. This difference in performance with pH may be related to a pH-dependent surface passivation layer or a difference in catalytic activity of the operational surface, although the latter is less likely given the lack of photocurrent transients in pH 10 electrolyte. The presence of current transients in pH 13 electrolyte, especially at potentials below 1 V *vs.* RHE suggest that surface optimization to promote catalytic activity and eliminate surface trap states could further improve both photocurrent and photovoltage. The apparent direct band gap from the direct-allowed Tauc signal is 2.35 eV. The substantial absorption tail, large photocurrent with 2.4 eV light source, and some photoresponse with 2.07 eV illumination suggest the presence of an indirect band gap closer to 2 eV. X-ray photoelectron spectroscopy (XPS, Fig. S3†) characterization after the pH 13 PEC measurements on Fig. 1 showed a near-surface Y/(Y + Fe) concentration of 0.47, slightly larger than the XRF (bulk) value of 0.33 in the as-synthesized film. Neither Y nor Fe is expected to corrode in strong alkaline electrolytes, and the stable photocurrent under the short duration measurements of Fig. 1 suggest this phase is an excellent candidate for stable photoanode operation.

PEC characterization of V_2CoO_6-tri (Fig. 2) in pH 9 electrolyte includes chopped illumination CA at 1.23 V *vs.* RHE, showing some current transients above the sustained photocurrent and photorepsonse down to 2.07 eV. An additional 30 minutes of chopped illumination with the 3.2 eV source indicates excellent stability of visible light photoresponse on this time scale, and the chopped illumination CV shows that the onset of photocurrent is below 0.73 V *vs.* RHE. XPS after PEC experiments (Fig. S4†) revealed near-surface Co/(Co + V) of 0.44, slightly higher than the XRF (bulk) value of 0.35 in the as-synthesized film. V is susceptible to corrosion, although this relatively minor alteration in near-surface composition, combined with the 30 min PEC stability measurement (Fig. 2a), suggest that the film is well passivated by a Co-rich oxide, similar to the passivation behavior of copper vanadate photoanodes.[20]

To put these 2 phases in the context of visible-active metal oxide photoanodes, we consider the 58 metal oxide phases for which we have observed photoanodic activity in our combinatorial experiments. Fig. 3 shows the 7 metal oxide phases with the highest external quantum efficiency (EQE) at 2.41 eV, which includes 2 discoveries from the present work, discoveries from our previous work,[15,16,21] and our reproduction of the previously-reported photoanodes $FeBiO_3$.[22] While EQE is amenable to

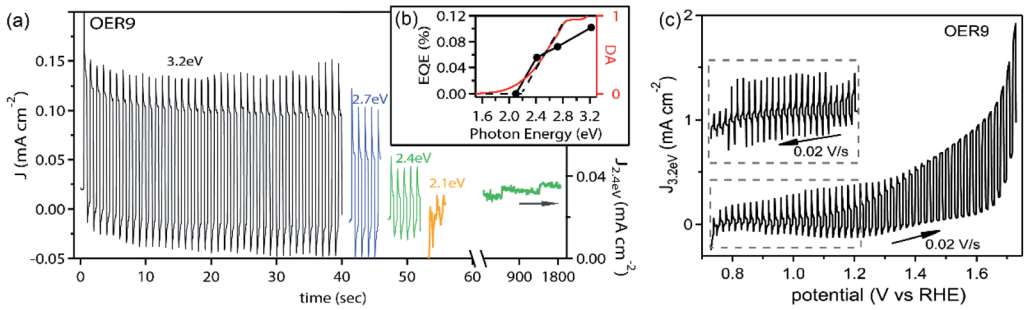

Fig. 2 Summary of toggled illumination PEC experiments on V_2CoO_6-tri where transition to higher (lower) current corresponds to toggling illumination on (off). (a) CA at 1.23 V *vs.* RHE in pH 9 electrolyte with 4 different light sources (left axis), and an additional 30 min with 2.4 eV illumination where an 11-illumination-cycle moving average of photocurrent is shown (right axis). (b) The corresponding spectral EQE (left axis) along with the UV-vis direct-allowed Tauc plot (right axis). (c) CV with cathodic sweep (inset) starting at 1.23 V *vs.* RHE and anodic sweep extending to 1.73 V *vs.* RHE.

Published on 31 January 2020. Downloaded by Lawrence Berkeley National Laboratory on 3/13/2020 3:43:11 PM.

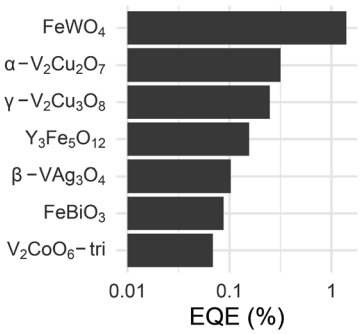

Fig. 3 The top 7 photoanodes by EQE at 2.41 eV from the database of 58 metal oxide photoanode phases (see ESI†). The photoanodes $Y_3Fe_5O_{12}$ and V_2CoO_6-tri reported herein are among the most promising phases due to their visible light photoactivity.

optimization, for example through tailoring carrier transport and catalyst coatings, the photon energy of photocurrent onset is more deeply engrained in the electronic structure of the metal oxide phase. After initial development,[23] years of optimization of $BiVO_4$ led to a 9-fold increase in external quantum efficiency for above-2.4 eV illumination,[24] whereas attempts to instil lower-energy activity have been relatively unsuccessful. The 7 metal oxide phases in Fig. 1 have higher EQE at 2.4 eV than $BiVO_4$ in our combinatorial experiments, so analogous improvements to these photoanodes could be particularly impactful due to their utilization of a larger portion of the solar spectrum. The remarkable performance optimization of $BiVO_4$ is concomitant with development of advanced computational and experimental techniques for understanding photodynamics, limiting aspects of carrier transport, electronic structure of heterogeneous surface layers, *etc.*, as recently reviewed by Yang *et al.*[25] Models of tandem-absorber photoelectrochemical cells indicate that lowering the photon energy onset for the photoanode from 2.4 eV to 2.07 eV could yield a 2-fold improvement in the solar to fuel conversion efficiency and is critical for achieving solar to fuel conversion efficiency in excess of 15%.[26] Per the "fail quickly" model introduced by Parkinson,[27] advanced characterization techniques should be applied to the materials described herein, which pass the critical criterion of visible light photoactivity but may suffer from other intrinsic properties that are not amenable to optimization *via* known materials engineering strategies.

Conclusions

Solar fuels photoanodes pose substantial challenges for materials discovery due to the combined needs of solar absorption, charge carrier separation and transport, oxidative stability, and catalytic activity for the OER. Combinatorial screening in composition spaces related to previous theory predictions as well as the photoanode literature resulted in the discovery of 29 metal oxide photoanodes, 15 with visible light response. This unprecedented success in photoanode discovery broadens the set of candidate materials for optimization and integration studies. The onset of photoactivity of V_2CoO_6-tri and $Y_3Fe_5O_{12}$, as well as 3 addition Y-containing metal oxides, near photon energy 2.07 eV make these phases of particular interest for further study to establish the next generation of metal oxide photoanodes for solar fuels technology.

Conflicts of interest

There are no conflicts to declare.

Acknowledgements

This material is based upon work performed by the Joint Center for Artificial Photosynthesis, a DOE Energy Innovation Hub, supported through the Office of Science of the U.S. Department of Energy under Award Number DE-SC0004993. Use of the Stanford Synchrotron Radiation Lightsource, SLAC National Accelerator Laboratory, is supported by the U.S. Department of Energy, Office of Science, Office of Basic Energy Sciences under Contract DE-AC02-76SF00515.

Notes and references

‡ Formula unit suffixes "hex", "orth", and "tri" are use to distinguish polytypes with hexagonal, orthorhombic, and trigonal crystal structures, respectively.

1 K. Sivula and R. van de Krol, *Nat. Rev. Mater.*, 2016, **1**, 15010.
2 F. F. Abdi and S. P. Berglund, *J. Phys. D: Appl. Phys.*, 2017, **50**, 193002.
3 S. Chu, W. Li, Y. Yan, T. Hamann, I. Shih, D. Wang and Z. Mi, *Nano Futures*, 2017, **1**, 022001.
4 H. He, A. Liao, W. Guo, W. Luo, Y. Zhou and Z. Zou, *Nano Today*, 2019, 100763, DOI: 10.1016/j.nantod.2019.100763.
5 J. H. Kim, Y. J. Jang, S. H. Choi, B. J. Lee, J. H. Kim, Y. B. Park, C.-M. Nam, H. G. Kim and J. S. Lee, *J. Mater. Chem. A*, 2018, **6**, 12693–12700.
6 M. Kölbach, I. J. Pereira, K. Harbauer, P. Plate, K. Höflich, S. P. Berglund, D. Friedrich, R. van de Krol and F. F. Abdi, *Chem. Mater.*, 2018, **30**, 8322–8331.
7 C.-M. Jiang, G. Segev, L. H. Hess, G. Liu, G. Zaborski, F. M. Toma, J. K. Cooper and I. D. Sharp, *ACS Appl. Mater. Interfaces*, 2018, **10**, 10627–10633.
8 M. Woodhouse, G. S. Herman and B. A. Parkinson, *Chem. Mater.*, 2005, **17**, 4318–4324.
9 J. G. Rowley, T. D. Do, D. A. Cleary and B. A. Parkinson, *ACS Appl. Mater. Interfaces*, 2014, **6**, 9046–9052.
10 T. F. Jaramillo, S. H. Baeck, A. Kleiman-Shwarsctein, K. S. Choi, G. D. Stucky and E. W. McFarland, *J. Comb. Chem.*, 2005, **7**, 264–271.
11 R. Gutkowski, C. Khare, F. Conzuelo, Y. U. Kayran, A. Ludwig and W. Schuhmann, *Energy Environ. Sci.*, 2017, **10**, 1213–1221.
12 R. Meyer, K. Sliozberg, C. Khare, W. Schuhmann and A. Ludwig, *ChemSusChem*, 2015, **8**, 1279–1285.
13 J. W. Lee, H. C. Ye, S. L. Pan and A. J. Bard, *Anal. Chem.*, 2008, **80**, 7445–7450.

 This journal is © The Royal Society of Chemistry 2020

Published on 31 January 2020. Downloaded by Lawrence Berkeley National Laboratory on 3/13/2020 3:43:11 PM.

14 Q. Yan, G. Li, P. F. Newhouse, J. Yu, K. A. Persson, J. M. Gregoire and J. B. Neaton, *Adv. Energy Mater.*, 2015, **5**, 1401840.

15 L. Zhou, Q. Yan, A. Shinde, D. Guevarra, P. F. Newhouse, N. Becerra-Stasiewicz, S. M. Chatman, J. A. Haber, J. B. Neaton and J. M. Gregoire, *Adv. Energy Mater.*, 2015, **5**, 1500968.

16 Q. Yan, J. Yu, S. K. Suram, L. Zhou, A. Shinde, P. F. Newhouse, W. Chen, G. Li, K. A. Persson, J. M. Gregoire and J. B. Neaton, *Proc. Natl. Acad. Sci. U. S. A.*, 2017, **114**, 3040–3043.

17 A. Shinde, S. K. Suram, Q. Yan, L. Zhou, A. K. Singh, J. Yu, K. A. Persson, J. B. Neaton and J. M. Gregoire, *ACS Energy Lett.*, 2017, 2307–2312, DOI: 10.1021/acsenergylett.7b00607.

18 E. Soedarmadji, H. S. Stein, S. K. Suram, D. Guevarra and J. M. Gregoire, *npj Comput. Mater.*, 2019, **5**, 79.

19 Y. Guo, N. Zhang, H. Huang, Z. Li and Z. Zou, *RSC Adv.*, 2017, **7**, 18418–18420.

20 L. Zhou, Q. Yan, J. Yu, R. J. R. Jones, N. Becerra-Stasiewicz, S. K. Suram, A. Shinde, D. Guevarra, J. B. Neaton, K. A. Persson and J. M. Gregoire, *Phys. Chem. Chem. Phys.*, 2016, **18**, 9349–9352.

21 L. Zhou, A. Shinde, S. K. Suram, H. S. Stein, S. R. Bauers, A. Zakutayev, J. S. DuChene, G. Liu, E. A. Peterson, J. B. Neaton and J. M. Gregoire, *ACS Energy Lett.*, 2018, **3**, 2769–2774.

22 X. Y. Chen, T. Yu, F. Gao, H. T. Zhang, L. F. Liu, Y. M. Wang, Z. S. Li, Z. G. Zou and J. M. Liu, *Appl. Phys. Lett.*, 2007, **91**, 022114.

23 K. Sayama, A. Nomura, Z. G. Zou, R. Abe, Y. Abe and H. Arakawa, *Chem. Commun.*, 2003, 2908–2909, DOI: 10.1039/b310428a.

24 K. R. Tolod, S. Hernandez and N. Russo, *Catalysts*, 2017, **7**, 13.

25 W. Yang, R. R. Prabhakar, J. Tan, S. D. Tilley and J. Moon, *Chem. Soc. Rev.*, 2019, **48**, 4979–5015.

26 K. T. Fountaine, H. J. Lewerenz and H. A. Atwater, *Nat. Commun.*, 2016, **7**, 13706.

27 K. Skorupska and B. A. Parkinson, in *Photoelectrochemical Solar Fuel Production From Basic Principles to Advanced Devices*, ed. S. Giménez and J. Bisquert, Springer International Publishing, Switzerland, 2016, pp. 427–462, DOI: 10.1007/978-3-319-29641-8.